ce/papers Proceedings in civil engineering

Ernst & Sohn A Wiley Brand

ORIGINAL ARTICLE

Load capacity of penstock manifolds subjected to increasing settlements at the vertical supports

Martin Langwieser | Alexander Ecker[1] | Harald Unterweger[1]

Correspondence

Dipl.-Ing. Martin Langwieser
Graz University of Technology
Institute of Steel Structures
Lessingstraße 25/III
8010 Graz, AUSTRIA
Email: langwieser@tugraz.at

[1] Graz University of Technology, Institute of Steel Structures, Graz, AUSTRIA

Abstract

Hydroelectric power plants usually have penstock manifolds near the powerhouse, including individual bifurcations to provide several turbines. These steel constructions have numerous vertical supports and are designed based on linear elastic behaviour, leading to very small allowable settlements at the supports.

For a representative built manifold, with five bifurcations (six branch pipes), the elastic-plastic load capacity was studied in detail, assuming dead load, internal pressure and increasing settlements at the supports. Different settlement patterns were studied. The development of plastic zones was analyzed, depending on the rate of settlement. Due to the high bending stiffness of the penstock manifold, the penstock detaches from the single supports due to the settlement, leading to a significant redistribution of the vertical reaction forces at the supports.

The comprehensive calculations show adequate robustness of the penstock manifolds, even though in case of very high settlements at the supports. Due to the significant redistribution of the reaction forces at the supports, these vertical supports must have an increased bearing capacity, in comparison to the reaction forces due to dead load and internal pressure based on linear elastic analyses.

Keywords

penstock, manifolds, settlement, load capacity

1 Introduction

This paper deals with the elastic-plastic load capacity of an existing penstock manifold, loaded with dead load (penstock and water infill) an internal pressure and increasing settlements at the supports. Penstock manifolds are built at the end of pressure shafts for hydroelectric storage powerplants to divide the water flow for different turbines or pumps. The pressure shaft with the subsequent manifold connects the water reservoir with the powerhouse. The manifold itself is composed of different bifurcations, which divide the water flow for different branch pipes (see Fig. 1). Manifolds are highly stressed components due to large internal pressure at the bottom near the powerhouse. They are expensive components and are designed for a long working live. Nevertheless, no systematic studies of the elastic-plastic load capacity were found in the literature by the authors, so this was the reason for these investigations. Also, in [1] the need of further investigations in this field is recorded.

Fig.1 shows the investigated geometry of the manifold for an existing storage powerplant. This powerplant was planned and built from 1965 to 1971. It has a design pressure at the manifold of p_i = 5,23 N/mm² (= 533 meter water head). For this hydroelectric powerplant, the water flow is divided by a big Y-branch pipe (not shown in Fig. 1) into two manifolds 1 and 2 (only the beginning of manifold 2 is shown in Fig. 1). Each of these manifolds has six branch pipes, which are anchored in the concrete wall of the powerhouse. So, both manifolds have fixed supports at the powerhouse and an upstream anchor point FP0 (see Fig. 1). Only manifold 1, with the shorter branch pipes, was investigated, because higher stresses occur due to the higher bending stiffness of the shorter branch pipes. The investigated manifold 1 is marked in yellow in Fig.1.

This manifold 1 is supported in vertical direction by 17 supports between the anchor point FP0 and the powerhouse, which allow displacements in both horizontal directions. These vertical supports are presumed to be frictionless in horizontal direction in the Finite-Element-Model, so they are called "frictionless supports". Six of these frictionless supports are located at the branch pipes. These six supports are coloured in blue in Fig.1. The others are coloured in green. The frictionless supports are designed as saddle supports (see cross-sections at G7 and G12 in Fig.1).

https://doi.org/10.1002/cepa.2565 wileyonlinelibrary.com/journal/cepa

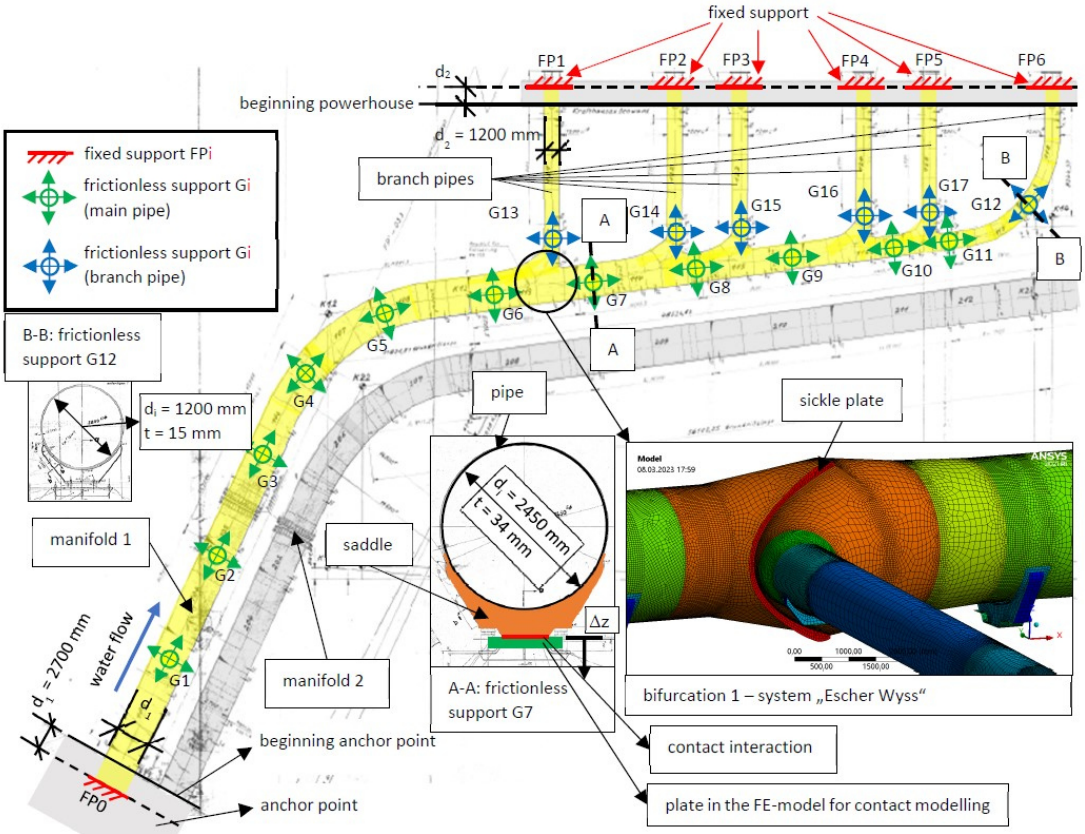

Figure 1 overview - penstock manifold of a hydroelectric powerplant with its supports

The manifold has its largest inner diameter d_1 = 2700 mm with a pipe thickness t = 32 mm at the anchor point. Downstream, the inner diameter of the pipes decreases step by step with the bifurcations. At the branch pipes, the smallest inner diameters (d_i = 1200 mm with a thickness t = 15 mm) can be found. The steel thickness t ranges from t = 98 mm at the sickle plates of the bifurcations (see Fig. 1) and t = 44 mm to t = 15 mm at the individual pipe plates. These bifurcations with inner sickle plates (see Fig. 1) are designed according to the so-called "Escher-Wyss" design concept (see bifurcation 1 in Fig. 1).

At that time, when this manifold was planned and constructed it was state of the art to calculate the whole manifold as a beam structure. So, the complex geometry of the manifold was simplified to a statically indeterminate beam model. At that time, it was not possible to investigate this system regarding to its elastic-plastic load capacity due to internal pressure and settlements with a Finite-Element-Analysis (FEA).

2 Methodology

2.1 FE-model of the whole manifold 1

The whole geometry of manifold 1 is modelled with shell elements. The reference surface of the shell elements is the inner surface of the pipes, the thickness is added to the outside of the shell. Only for the sickle plates of the bifurcations the reference surface of the shell elements is the middle surface of the plate. The saddles of the frictionless supports are also defined as shells.

In the FE-model, the fixed supports are not located at the beginning of the powerhouse wall, they are moved one diameter of the branch pipe into the powerhouse wall (see Fig. 1). The reason for that is, that the theoretical fixed support of the real branch pipes is not at the beginning of the powerhouse wall, because of the flexibility of the concrete. The same approach is used at the upstream anchor point FP0 (see Fig. 1).

The saddles of the frictionless supports are welded to the pipe, so the connection between the manifold and the saddles is fixed. To implement a settlement and a "lift off" behaviour of the frictionless supports (only compressive forces are transferable), rigid plates are modelled under the saddles and a contact interaction (frictionless "hard" contact) between the saddles and the rigid plates at the foundations is implemented (see Fig. 1). These rigid plates (green plate under the saddle in Fig. 1) are forced down in the FEA to simulate a settlement Δz.

The element order of the used shell elements for the whole model is defined as quadratic. The shape of the shell elements is quadrilateral for most elements. The maximum length of the elements is defined between 100 mm and 250 mm. Mesh refinements are done, where stress concentrations are expected. So, the shell edges at the bifurcations (s. Fig.1), at the fixed supports and at the mitre bends are refined. The element lengths of the refined areas correspond approximately to the shell thickness t. For example, the defined element length at the shell edges at the bifurcation 1 is about 40 mm.

The material of the manifold is a steel named Aldur 45/60, except of the sickle plates. These are made of steel Aldur 58. The saddles of the manifold are made of a steel St37. For the material Aldur 45/60 the yield stress (nominal value) is given by 450 N/mm². The Aldur 58 has a reduced yield strength of 380 N/mm² due to the sickle plate thickness of 98 mm and for the St37 the yield strength is

235 N/mm².

All three materials are defined with an elastic-plastic bilinear material behaviour. A young's modulus of E = 210000 N/mm² and a poisson's ratio of v = 0.3 are provided for the elastic behaviour. After reaching the yield strength, a tangent modulus is defined with a low gradient of E/100 to receive a better calculation performance.

2.2 Definition of the load cases and the loading procedure

Overall, nine different load cases (LC) are investigated for the manifold 1 (LC0, LC0*, LC1, LC2, LC2*, LC3, LC4, LC5 and LC5*). In these nine load cases different load combinations or supporting conditions are investigated. All load cases include an internal pressure, so geometrical imperfections are negligible due to the smoothing effect of the internal pressure. The load cases marked with an asterisk (*) have the same load combination, but the frictionless supports at the branch pipes (marked in blue in Fig. 1) are left out (not active). The reason for that is explained in chapter 3.2.

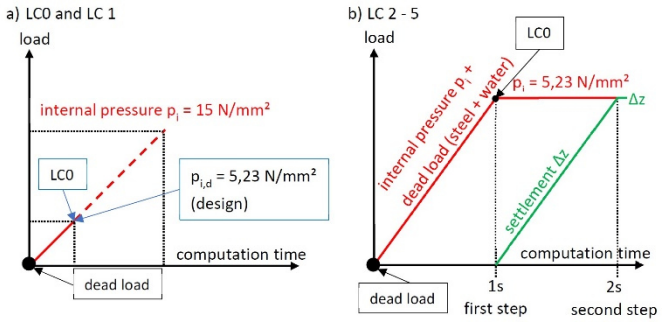

Figure 2 loading procedure in the FEA for the different load cases
a) LC0 - LC1: dead load and internal pressure
b) LC2 – LC5: dead load, internal pressure (design) plus settlement Δz

The first load case LC0 is defined as a reference load case. In this load case LC0 the dead load (weight of the steel manifold plus the water inside) and the design pressure (p_i = 5.23 N/mm²) are applied as shown in Fig. 2a and 2b. In load case LC1 (s. Fig. 2a) the internal pressure is increased up to 15 N/mm². So, the reserves due to the material plasticity for a higher internal pressure than the design pressure are investigated. In load cases LC2 to LC5 different settlements are investigated. Therefore, the starting point in the FEA for the settlements Δz is always LC0, as shown in Fig. 2b, or LC0* for the inactive branch pipe supports. So, different settlements are applied after loading the model with the dead load and the design pressure (s. Fig. 2b). In load case LC2 a settlement of the powerhouse is simulated. All fixed supports FP1 to FP6 (see. Fig. 1) are forced down with a maximum settlement of Δz = 200 mm. This is an unusual high settlement, but it was the intention to show the full plastic capacity of the manifold 1. For comparison with LC2, the same procedure is done in the load case LC2* with inactive frictionless supports at the branch pipes. In load case LC3, only the fixed support FP1 is forced down with a settlement of Δz = 200 mm and in load case LC4 the same procedure was applied for the fixed support FP5.

Finally, settlements at the frictionless supports were investigated. Therefore, the bearing plates under the frictionless supports G7 and G8 (see Fig. 1) are forced down. In load case LC5 this settlement is simulated at the original support conditions of the manifold 1 and in load case LC5* the same procedure is done without the frictionless supports at the branch pipes.

The FEA all of these load cases provided three different non-linearities, which are, i) the bilinear material behaviour, ii) the non-linear contact behaviour at the saddle supports and, iii) the non-linear geometry behaviour (calculation with large deflections). Therefore, the loads of the internal pressure and the settlements are applied in small steps between 0.5 % and 10 % of the total loads till reaching the total loads.

3 Results for the elastic-plastic FEA

3.1 Results for the load case LC1 - internal pressure

As mentioned before, in load case LC1, the internal pressure is increased up to p_i = 15 N/mm² (see Fig. 2a). This is almost three times higher than the design pressure p_i = 5.23 N/mm² and should show the plastic load capacity of this manifold. Fig. 3 shows the internal pressure p_i of the Finite-Element-Analysis (FEA), depending on the maximum equivalent plastic strain $\varepsilon_{pl,equ}$ at the manifold. The equivalent plastic strain $\varepsilon_{pl,equ}$ is the most important value to evaluate the plastic load capacity. Different significant internal pressures p_i are marked in Fig. 3. Fig. 3 shows, that nearly no plastic strains occur at the design pressure ($p_{i,d}$ = 5.23 N/mm²). This confirms the appropriate elastic design in the 1970s, when the manifold was designed. Another pressure, marked in Fig. 3, is the internal pressure $p_{i,\varphi,450,min}$. This pressure stands for the smallest capacity of the straight pipe sections in the manifold, ignoring any longitudinal stresses (hoop stress σ_φ reaches the yield stress f_y), according to: $p_{i,\varphi,450,min} = \min[f_y \cdot t_i / (d_{m,i} / 2)] = \min[450 \cdot t_i / (d_{m,i} / 2)]$, where d_m is the mean diameter of the pipe. The decisive pipe section is the main pipe with d_m = 2732 mm and t = 32 mm. This yields to the pressure $p_{i,\varphi,450,min}$ = 10.54 N/mm² in Fig. 3. It is expectable that the plastic strains grow larger above this pressure due to the beneficial longitudinal stresses σ_x and the strain hardening.

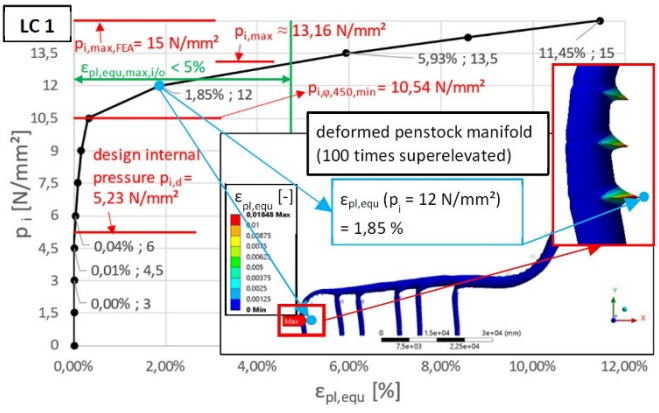

Figure 3 Results of load case 1 (LC1) – equivalent plastic strains ($\varepsilon_{pl,equ}$) due to the increase of the internal pressure

The maximum allowable pressure $p_{i,max}$ is defined where $\varepsilon_{pl,equ}$ reaches 5 %. This 5 % plastic strain is a common limit value for the plastic load capacity (according to [2]). The maximum allowable pressure $p_{i,max}$ = 13.16 N/mm², which is 150 % higher than the design pressure $p_{i,d}$, shows the unexpected high plastic load capacity of the manifold. Fig. 3 also shows the deformed shape (100 times super-elevated) with the maximum plastic strain $\varepsilon_{pl,equ} = 1{,}85\,\%$ at the mitre bend for p_i = 12.0 N/mm².

3.2 Results for the load cases LC2, LC3 and LC4 - settlements at the powerhouse

In this chapter the results for different settlements at the fixed supports FP1 - FP6 at the powerhouse (see Fig. 1) are shown. Fig. 4 shows the deformed shape (25 times super-elevated) of the manifold with the vertical deformation (z-direction) for the LC2. In LC2, all fixed supports FP1 – FP6 at the powerhouse are forced down by Δz = 200 mm. This is an unusual high settlement, but it was the intention to show the full plastic load capacity of the manifold. Due to the supports at the branch pipes (frictionless supports G12 – G17) and the settlement at the powerhouse, an uplift of the main pipe occurs, which is shown in Fig.4. Large stresses and plastic strains occur at the supports of the branch pipes (G12 – G17) and at the fixed supports at the powerhouse (FP1 – FP6) due to the large settlement.

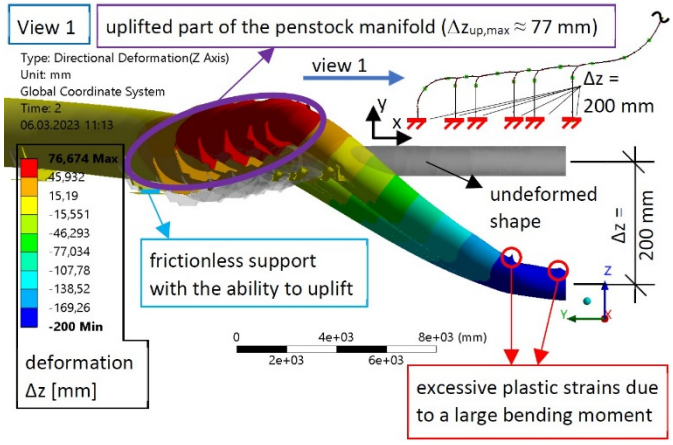

Figure 4 Load Case 2 (LC2) - side view of the deformed manifold; vertical deformations due to a settlement of Δz = -200 mm at the fixed supports of the powerhouse (all branches)

So, in Fig. 4 it becomes obvious, that for settlements at the powerhouse, the supports G12 – G17 of the branch pipes increase the constraining forces and stresses in the manifold. These supports (G12 – G17) at the branch pipes are not really necessary for the dead load plus internal pressure and could be left out. In general, the dead load leads to very small stresses in the manifold. So, this was the reason for load case LC2*, where the supports G12 – G17 are inactive. A comparison of the equivalent plastic strains $\varepsilon_{pl,equ}$ for LC2 and LC2*, depending on the settlement value Δz, shows Fig. 5. The highest strains $\varepsilon_{pl,equ}$ for LC2 and LC2* occur at the saddle supports (G12 for LC2 and G11 for LC2*), as shown in Fig. 5. The strains $\varepsilon_{pl,equ}$ for LC2* are significantly smaller than for LC2, especially for Δz = 40 mm (88 % smaller) and Δz = 60 mm (72 % smaller).

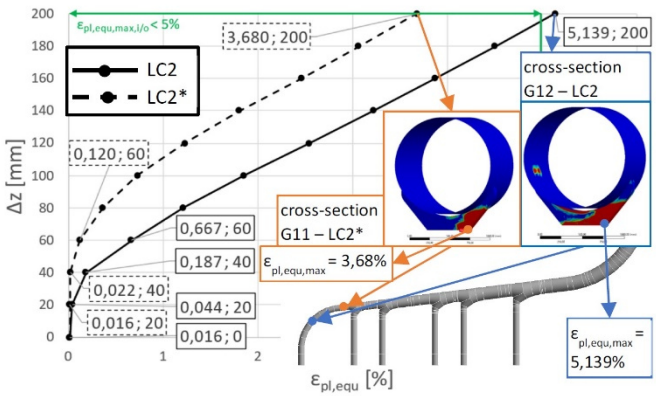

Figure 5 Load Case 2 (LC2 and LC2*) - equivalent plastic strains $\varepsilon_{pl,equ}$ due to the increased settlement Δz of the fixed supports at the powerhouse

Fig. 6 shows the reaction bending moments M_{y^*} (about horizontal cross-section axis y*, see Fig. 6) at the fixed supports for FP1 and FP5, depending on the settlement value Δz. Fig. 6 shows also the comparison of the moments M_{y^*} for LC2 and LC2*. As expected, the moments M_{y^*} for LC2* are lower for the same settlement value, compared to LC2. The moments M_{y^*} for the other load cases LC3 (only FP1 is forced down) and LC4 (only FP5 is forced down) are also shown in Fig. 6. The highest moments M_{y^*} were reached for the settlement of a single fixed support at FP1 or FP5.

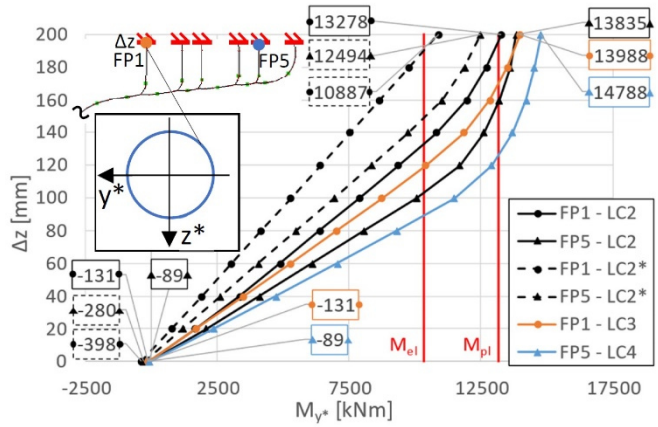

Figure 6 Load Case LC2-LC4 – bending moments M_{y^*} at the fixed supports of the powerhouse due to the increased settlement Δz at the powerhouse

The red lines in Fig.6 show the bending moment capacity for uniaxial bending of the pipe cross-section at the fixed supports (d_i = 1200 mm and t = 20 mm). The elastic bending moment capacity M_{el} was calculated with the elastic section modulus (M_{el} = 10355 kNm). The plastic bending moment capacity M_{pl} was determined by using the elastic capacity M_{el} and a shape coefficient. This shape coefficient represents the ratio (M_{pl} / M_{el} =4/π → M_{pl} = 13181 kNm).

As shown in Fig.6 for the load cases LC2, LC3 and LC4 reaction moments above the uniaxial plastic moment capacity M_{pl} occur. These moments, higher than M_{pl}, are only possible due to the fixed supports and the multiaxial stress state in the pipe.

3.3 Results for the load case LC5 - settlements at the frictionless supports

In this chapter, the load carrying behaviour of the manifold due to a settlement of two supports at the main pipe is presented. As mentioned in section 2, for both load cases LC5 and LC5*, the bearing plates under the saddle (see Fig. 1) G7 and G8 are forced down. The difference between load case LC5 and LC5* is the left out of supports at the branch pipes for LC5*. When the bearing plate, which is connected with a frictionless contact interaction to the saddle (see Fig. 1), is forced down with Δz, the pipe can be detached from the saddle. This is called "lift off".

Fig. 7 shows the changes of the vertical reaction forces of the surrounding supports due the settlement of the frictionless supports G7 and G8. The vertical reaction forces at Δz = 0 are coming from the dead load and the internal pressure (LC0). Fig. 7 shows, that "lift off" occurs at about Δz = 2.2 mm for support G8 and at Δz = 3.2 mm for support G7. The vertical forces for the surrounding supports G6, G9, G13, G14 and G15 are increasing significantly due to the settlement. When "lift off" of the supports G7 and G8 occur, the vertical reaction forces don't change anymore.

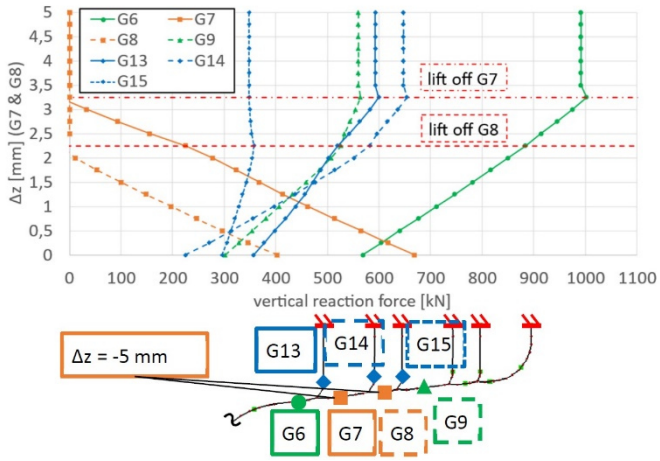

Figure 7 Load case 5 (LC5), vertical settlement at G7 and G8 - vertical reaction forces at the frictionless supports, due to increased settlements Δz

Fig. 7 shows, that the manifold has a very high bending stiffness, so "lift off" at the supports occurs at very small settlements (2 – 3 mm). Also, the changes of the strains and stresses in the pipes of the manifold due to the settlement of the supports G7 and G8 are very small and no plastic strains occur, so they are not documented here.

The same settlements of the supports G7 and G8 and the changes of the vertical reaction forces of the surrounded supports are also investigated for LC5* in Fig.8. It can be seen, that the "lift off" at both supports G7 and G8 happened at the same settlement value of Δz = 7.5 mm. So larger settlements, compared to LC5, can occur until "lift off". The nearest supports G6 and G9 undergo an increase of their reaction forces, whereas the reaction forces of the following frictionless supports G5 and G10 decrease. So, this load carrying behaviour of the manifold is comparable with that of a continuous beam.

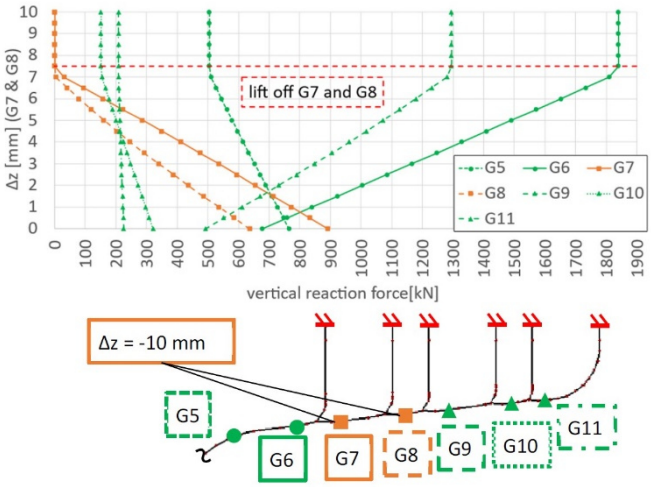

Figure 8 Load case 5* (LC5*), vertical settlement at G7 and G8, without branch supports - vertical reaction forces at the frictionless supports, due to increased settlements

Table 1 dimensions of the pipe at the frictionless supports and vertical reaction forces for dead load plus design pressure (LC0 and LC0*) and dead load, design pressure plus settlement of the supports G7 and G8 (LC5 and LC5*) after "lift off"

support	d_i [mm]	t [mm]	d_i/t	LC 0	LC 5	LC 0*	LC 5*
				F_v [kN]	F_v [kN]	F_v [kN]	F_v [kN]
G5	2700	34	79	720	580 (-19 %)	765	505 (-34 %)
G6	2700	34	79	569	992 (+74 %)	677	1840 (+172 %)
G7	2450	34	72	669	lift off (-100 %)	892	lift off (-100 %)
G8	2200	36	61	402	lift off (-100 %)	636	lift off (-100 %)
G9	1950	25	78	302	560 (+85 %)	493	1295 (+163 %)
G10	1600	28	57	211	245 (+16 %)	321	151 (-53 %)
G11	1200	25	48	27	39 (+44 %)	225	209 (-7 %)
G13	1200	25	48	357	593 (+66 %)	-*	-*
G14	1200	25	48	224	647 (+189 %)	-*	-*
G15	1200	25	48	296	349 (+18 %)	-*	-*

*frictionless supports at the branch pipes inactive

Table 1 shows now the comparison of the vertical reaction forces for these two load cases LC5 and LC5* (after "lift off") with the vertical reaction forces of the reference load cases LC0 and LC0*. These reference load cases show the reaction forces due to the applied dead load and design pressure $p_{i,d}$. Table 1 also shows the inner diameter d_i of the pipe, the shell thickness t and the ratio d_i/t for the cross-section of the pipe at the support shown. The percentage value, underneath the reaction forces of LC5 and LC5*, shows the difference to the reaction forces of the reference load cases LC0 and LC0*. Table 1 shows, that the closest supports to G7 and G8 gained the highest additional reaction forces.

4 Discussion of the results

4.1 Load case LC1 – increase of the internal pressure

LC1 showed, that an unexpected large plastic load capacity of the manifold is available, especially for the bifurcations and the mitre bends. Relevant equivalent plastic strains $\varepsilon_{pl,equ}$ occur only after reaching the internal pressure $p_{i,\varphi,450,min}$ for the straight pipes (see Fig. 3). As shown in Fig.3, the maximum values $\varepsilon_{pl,equ}$ appeared first on the inside of the mitre bends. This behaviour is consistent with the fact, that at this position stress concentrations appear as investigated in studies of Green & Emmerson [3] and Ecker [4].

Another interesting fact is, that all these large plastic strains $\varepsilon_{pl,equ}$ in Fig. 3 appeared either in the mitre bends or in the straight pipes of the manifold. The bifurcations showed even in the last calculated step (with p_i = 15 N/mm²) very small plastic strains $\varepsilon_{pl,equ}$. This is consistent with the original design in the 1970s for the bifurcations. The bifurcations had a higher safety level in the design as the straight pipes and the mitre bends.

4.2 Load cases LC2, LC3 and LC4 – settlements at the powerhouse

The investigations of LC2 to LC4 showed, that very high settlements of Δz = 200 mm at the powerhouse could occur without significant plastic strains at the manifold, even though the design pressure ($p_{i,d}$ = 5.23 N/mm²) is active. But these load cases also showed, that very high reaction moments M_{y*} occur at the fixed supports at the powerhouse (see Fig. 6). It is questionable if the concrete of the powerhouse wall can resist these high stresses from the reaction moments. These load cases also showed, that the supports at the branch pipes (G12 – G17, see Fig. 1) significantly increase the constraining forces and stresses in the manifold due to the settlement of the powerhouse. So, the plastic strains $\varepsilon_{pl,equ}$ could be under the 5 %-boundary (for Δz = 200 mm) if the supports at the branch pipes (G12 – G17) would be set inactive like in LC2*. It was also investigated, that these supports (G12 – G17) are not really necessary for the dead load plus internal pressure and they can be left out. In general, the dead load leads to very small strains and stresses in the manifold. It should be mentioned, that settlements in general lead to secondary stresses (according to [2]) and these stresses can be limited through yielding of the steel.

4.3 Load case LC5 – settlements at the frictionless supports of the penstock manifold

The FEA investigations for LC5 and LC5* show, that the settlement of the frictionless supports (G7 and G8) causes a "lift off" of the pipe at these supports (see Fig. 7 and 8) at very small settlement values (Δz ≈ 3 mm for LC5 and Δz ≈ 7.5 mm for LC5*). This is based on a very high bending stiffness of the manifold. So, the reaction forces at the supports of the manifold are very sensitive to settlements, but the FEA didn't show any plastic strains $\varepsilon_{pl,equ}$ for the load cases LC5 and LC5*. The reason for that is, that the saddle supports are constructed in such a way, that they have enough elastic load capacity left for these additional reaction forces (see Fig. 6 and 7) due to the settlements. This is the right way to design the supports of such a manifold with a high bending stiffness. Due to the small distance between the vertical supports the additional stresses in the manifold due the "lift off" at the supports G7 and G8 are also quite small.

5 Conclusion

In this paper, the elastic-plastic behaviour of an existing penstock manifold was investigated with different load cases. It was shown that significant plastic reserves are available for manifolds. The penstock manifold also shows plastic reserves at the mitre bends and at the bifurcations for an applied internal pressure. There were internal pressures more than 2 times higher than the design pressure possible, because of these plastic load capacities. For settlements at the powerhouse, it was shown, that the supports at the branch pipes increased the constraining stresses in the manifold due to the powerhouse settlements. So, the plastic strains $\varepsilon_{pl,equ}$ could be reduced by inactivating the branch pipe supports. It was investigated, that these are not really necessary for the dead load and internal pressure. For settlements at the frictionless supports it was shown, that the manifold has a very high bending stiffness and small settlement values caused "lift off" at the supports and large changes in the vertical reaction forces. So, it is necessary to design robust supports, which can carry additional vertical forces due to possible settlements. For this investigated manifold, the supports with the saddle design had provided enough capacity reserves, so the reaction forces could be doubled without plastic strains. Therefore, these settlements didn't limit the load carrying behaviour of the manifold.

6 Acknowledgements

The authors would like to thank the project-partners Andritz Hydro, Bilfinger Industrial Services, Illwerke vkw, Kelag, ÖBB Infrastruktur, TIWAG – Tiroler Wasserkraft and Verbund Hydro Power for the good cooperation and the financial support of this research project [5]. The support of Österreichs Energie and the Austrian research fund FFG is also gratefully acknowledged.

References

[1] Taras A.; Kager A.; Theiner D.; Cavedon.V. (2020) *Zustandsbewertung bestehender Druckrohrleitungen von Wasserkraftanlagen*. Stahlbau 89, H. 5, S.424-438. https://doi.org/10.1002/stab.202000012

[2] Eurocode 1993-1-6 (2017), *Eurcode 3: Design of steel structures*, Part 1-6: Strength and Stability of Shell Structures.

[3] Green A.E., Emmerson W.C. *Stresses in a pipe with a discontinous bend*. J.Mechs. Phys. Solids. Vol.9 1961

[4] Ecker A. (2012), *Elastoplastisches Tragverhalten von Segmentkrümmern bei Innendruckbelastung*. master thesis, TU Graz

[5] Unterweger H., Ecker A., Langwieser M. (2023) *Trag- und Verformungsverhalten von Verteilrohrleitungen*. FFG–research project, technical report (not published)